

Dynamical chaos and power spectra in toy models of heteropolymers and proteins

Mai Suan Li,^{1,2} Marek Cieplak,¹ and Nazar Sushko¹

¹*Institute of Physics, Polish Academy of Sciences, Aleja Lotnikow 32/46, 02-668 Warsaw, Poland*

²*Institut für Theoretische Physik, Universität zu Köln, Zùlpicher Straße 77, D-50937 Köln, Germany*

(Received 5 April 2000)

The dynamical chaos in Lennard-Jones toy models of heteropolymers is studied by molecular dynamics simulations. It is shown that two nearby trajectories quickly diverge from each other if the heteropolymer corresponds to a random sequence. For good folders, on the other hand, two nearby trajectories may initially move apart but eventually they come together. Thus good folders are intrinsically nonchaotic. A choice of a distance of the initial conformation from the native state affects the way in which a separation between the twin trajectories behaves in time. This observation allows one to determine the size of a folding funnel in good folders. We study the energy landscapes of the toy models by determining the power spectra and fractal characteristics of the dependence of the potential energy on time. For good folders, folding and unfolding trajectories have distinctly different correlated behaviors at low frequencies.

PACS number(s): 87.15.-v, 71.28.+d, 71.27.+a

I. INTRODUCTION

The notion of chaos in physical systems has several meanings. For instance, in the context of spin glasses it refers to the phenomenon of instability of the ground state against weak perturbations in the exchange couplings [1]. In the context of dynamical systems, on the other hand, it refers to an acute sensitivity of trajectories to the initial conditions. Both of these meanings have relevance for understanding proteins and random heteropolymers.

In sequences of aminoacids, the static chaos can be probed by investigating how mutations affect the stability of the ground state. Several studies [2–4] have demonstrated that the native state of a random heteropolymer is unstable against mutations whereas there is stability in designed sequences provided the lengths of the sequences, N , are sufficiently small. It should be noted that the mutations may have a strong effect on folding kinetics even in the case of short proteins [5]. Investigation of the effects of an aminoacid substitution in a protein is an essence of experimental procedures aimed at determining the transition state in folding [6].

Here we focus on the notion of dynamical chaos in such systems and ask how do two folding trajectories relate to each other as the system evolves from two nearby conformations. Furthermore, can such information provide clues about the nature of the energy landscape of the system?

We consider continuum space models, as opposed to lattice models, since the latter have intrinsically discretized dynamics of a rather arbitrary nature. Specifically, we consider three toy $N=16$ off-lattice models that have been extensively characterized before [7–9] and whose native states are shown in Fig. 1. The Hamiltonians of these systems are defined in terms of the Lennard-Jones potentials (see Sec. II) and the time evolution is determined by Newton's equations that are solved by using the methods of molecular dynamics [10]. The first two of these systems, denoted in [7,8] as G and R' , are two dimensional whereas the third, denoted by H , is a Go-like model [11] of a three-dimensional helix [9]. The quality of folding of these systems has been determined by using thermodynamic [12] and kinetic [13] criteria.

Among the three systems, G is found to be a good folder, R' is a bad folder, and H has intermediate folding properties. Thus G is an analog of a protein and R' corresponds to a typical random heteropolymer and H is a borderline case. The task of this paper is to compare the chaos-related properties across this range of foldability.

As a measure of the distance between two conformations a and b we take δ_{ab} where

$$\delta_{ab}^2 = \frac{1}{N^2 - 3N + 2} \sum_{i \neq j, j \pm 1} (|\vec{r}_i^a - \vec{r}_j^a| - |\vec{r}_i^b - \vec{r}_j^b|)^2, \quad (1.1)$$

and where \vec{r}_i^a is the position vector of the i th monomer in the conformation a . This distance involves relative distances between the monomers and is bounded due the finite spacial extent of any conformation. Thus this distance cannot diverge as time grows which makes the characterization of the dynamical chaos unconventional in this case.

Notice that once the system folds from a random conformation to the native state, it may either stay in the immediate vicinity of the native state or it may depart further away and then keep visiting the native state. This translates into two possible scenarios for the asymptotic behavior of δ_{ab} : either the distance saturates asymptotically at a finite value—the case of H and R' , or it tends to zero—the case of G . Thus good folding properties are reflected in the small asymptotic values of δ_{ab} which may be used as an alternative criterion for good foldability. The asymptotic saturation of δ_{ab} in bad folders is achieved at a much shorter time scale than one

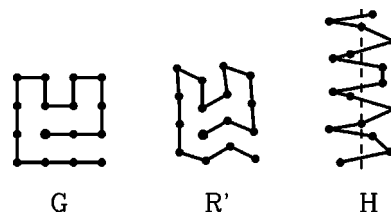


FIG. 1. Native conformations of three sequences studied in this work.

needed to establish the asymptotic tendency in a good folder. Thus the bad folders can be said to be more chaotic than the good folders.

Studies of the distance between two trajectories provide information about the energy landscape available to a sequence. Complementary information can be obtained by studying individual trajectories. This is shown in Sec. IV where we consider fractal and spectral properties of the potential energy curve, $E_p(t)$, as seen on a trajectory as a function of time t . The power spectrum, obtained by Fourier transforming $E_p(t)$, is found to indicate a correlated noise pattern and it shows sensitivity to a sequence in a way which is consistent with H being intermediate. Furthermore, the corresponding low-frequency power-law exponent is found to be markedly different for folding and unfolding trajectories in systems of good foldability. The fractal dimensionality of the $E_p(t)$ curve is determined according to a procedure developed in [14,15]. We find that, for the well-folding system, the temperature dependence of this fractal dimensionality has a dip around a temperature which is optimal for folding. No such dip arises in poor folders.

II. THE SEQUENCES

We start our discussion by defining models that we study. The sequences denoted by G and R' are two-dimensional versions of the model introduced by Iori, Marinari, and Parisi [16]. Their native states are shown in Fig. 1. The Hamiltonian is given by

$$H = \sum_{i \neq j} \left\{ k(d_{i,j} - d_0)^2 \delta_{i,j+1} + 4\epsilon \left[\frac{C}{d_{i,j}^{12}} - \frac{A_{ij}}{d_{i,j}^6} \right] \right\}, \quad (2.1)$$

where i and j range from 1 to $N=16$. The distance between the beads $d_{i,j}$ is defined as $|\vec{r}_i - \vec{r}_j|$, where \vec{r}_i denotes the position of bead i . d_{ij} is measured in units of σ , the typical value of which is $\sigma=5 \text{ \AA}$. The harmonic term in the Hamiltonian, with the spring constant k , couples the beads that are adjacent along the chain. The remaining terms represent the Lennard-Jones potential. In [16], $A_{ij}=A_0 + \sqrt{\beta} \eta_{ij}$, where A_0 is constant and η_{ij} 's are Gaussian variables with zero mean and unit variance; β controls the strength of the quenched disorder. The case of $\eta_{ij}=0$ and $A_0=C$ would correspond to a homopolymer with the standard Lennard-Jones interaction used in the simulations of liquids. In Eq. (2.1) ϵ is the typical Lennard-Jones energy parameter. We adopt the units in which $C=1$ and consider k to be equal to 25ϵ . Smaller values of k may violate the self-avoidance of the chain [7]. The coupling constants A_{ij} for system R' are listed in Ref. [7]. These are shifted Gaussian-distributed numbers with the strongest attracting couplings assigned to the native contacts. For system G , A_{ij} is taken to be 1 or 0 for the native and non-native contacts, respectively. System R' has been shown to be structurally overconstrained and hard to fold.

The helical system H has a native state, shown in Fig. 1, that mimics typical α -helix secondary structures. In this case the distances between beads are assumed to have the length $d_0=3.8 \text{ \AA}$. As one proceeds along the helix axis from one bead to another, the bead's azimuthal angle is rotated by

100° and the azimuthal length is displaced by 1.5 \AA . The Hamiltonian used to describe the helix is a Go-like modification of Eq. (2) and it reads [9]

$$H = V^{BB} + V^{NAT} + V^{NON}. \quad (2.2)$$

The first term is a backbone potential which includes the harmonic and anharmonic interactions

$$V^{BB} = \sum_{i=1}^{N-1} [k_1(d_{i,i+1} - d_0)^2 + k_2(d_{i,i+1} - d_0)^4]. \quad (2.3)$$

We take $d_0=3.8 \text{ \AA}$, $k_1=\epsilon$, and $k_2=100\epsilon$. The interaction between residues which form native contacts in the target conformation is chosen to be of the Lennard-Jones form

$$V^{NAT} = \sum_{i < j}^{NAT} 4\epsilon \left[\left(\frac{\sigma_{ij}}{d_{ij}} \right)^{12} - \left(\frac{\sigma_{ij}}{d_{ij}} \right)^6 \right]. \quad (2.4)$$

We choose σ_{ij} so that each contact in the native structure is stabilized at the minimum of the potential, i.e., $\sigma_{ij} = 2^{-1/6} d_{ij}^N$, where d_{ij}^N is the length of the corresponding native contact. Residues that do not form the native contacts interact via a repulsive soft-core potential V^{NON} , where

$$V^{NON} = \sum_{i < j}^{NON} V_{ij}^{NON}, \quad (2.5)$$

$$V_{ij}^{NON} = \begin{cases} 4\epsilon \left[\left(\frac{\sigma_0}{d_{ij}} \right)^{12} - \left(\frac{\sigma_0}{d_{ij}} \right)^6 \right] + \epsilon, & d_{ij} < d_{cut} \\ 0, & d_{ij} > d_{cut}. \end{cases} \quad (2.6)$$

Here $\sigma_0 = 2^{-1/6} d_{cut}$, $d_{cut} = 5.5 \text{ \AA}$.

The time evolution of the sequences is determined by the fifth-order predictor-corrector scheme [10]. The integration step is chosen to be 0.005τ , where $\tau = m\sigma^2/\epsilon$ is the characteristic time unit and m is the mass of a bead. In order to simulate systems in contact with a heat bath of temperature T , we augment the equations of motion by the Langevin uncorrelated noise terms as described in [9],

$$m\ddot{\mathbf{r}} = -\Gamma \dot{\mathbf{r}} + F_c + \eta, \quad (2.7)$$

where $F_c = -\nabla_r E_p$ and

$$\langle \eta(0) \eta(t) \rangle = 2\Gamma k_B T \delta(t), \quad (2.8)$$

where k_B is the Boltzmann constant. We take Γ equal to 2. In the following, the temperature will be measured in the reduced units of ϵ/k_B .

Figure 2 shows the T dependence of folding times for the three sequences studied. The folding time is defined as the median first passage time and the folding is declared to be accomplished if the distance to the native state δ_{n_s} becomes smaller than the native basin size δ_c . δ_c is defined by the shape distortion method [8] and it is equal to $(0.2 \pm 0.01)\sigma$ and $(0.09 \pm 0.01)\sigma$ for sequence G and R' , respectively. For sequence H , $\delta_c = (0.6 \pm 0.05) \text{ \AA} = (0.12 \pm 0.01)\sigma$.

The folding is the fastest at the temperature T_{min} below which glassy kinetics set in. We determine that $T_{min} = 0.15 \pm 0.02$, 0.4 ± 0.02 , and 0.3 ± 0.02 for G , R' , and H , respec-

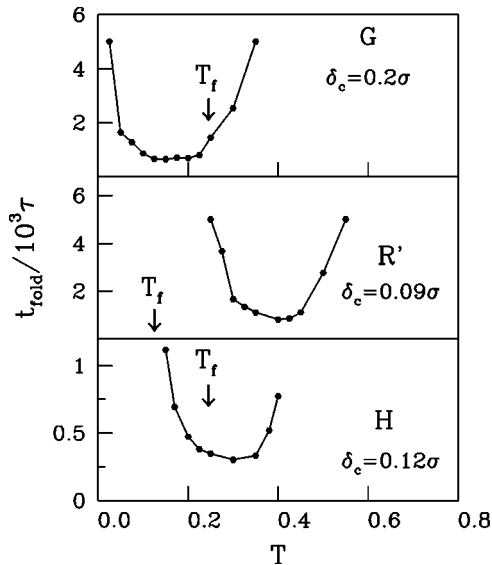


FIG. 2. The temperature dependence of the folding times for sequences G , R' , and H . The results are based on 100 starting random conformations. The arrows indicate the folding temperatures.

tively. Similar estimates of T_{min} were obtained with a Monte Carlo ‘‘dynamics’’ [7] (at a larger CPU cost).

Socci and Onuchic [13] have proposed that what determines good foldability is whether the folding temperature T_f is outside of the range of temperatures where kinetics become glassy. T_f is defined as a temperature at which the equilibrium probability of being in the native state is 1/2. Here, we rephrase this criterion in the following way: a sequence is a good folder if T_f is greater than T_{min} , otherwise foldability is bad. We determine T_f through a Monte Carlo process and get values indicated by the arrows in Fig. 2. The relative values of T_{min} and T_f indicate what was announced in Sec. I: G is a good folder, H is intermediate, and R' is a bad folder. Characterization based on the specific heat and structural susceptibility yields a similar conclusion [7–9].

Another relevant property of a sequence is its characteristic funnel size δ_f . It can be estimated by generating random conformation of the system and then quenching them (by setting $T=0$) and determining whether the resulting quenched state is native or not [8]. This allows one to estimate the probability P of getting to the native state from a conformation which is δ away from the native state. The critical value of δ , δ_c above which this probability becomes smaller than one may be identified as a characteristic δ_f . Our results on P are shown in Fig. 3 from which we can deduce that $\delta_f \approx 0.55\sigma$, 0.35σ , and 0.16σ for G , R' , and H , respectively (for H we took $\sigma = 5 \text{ \AA}$). Thus the good folder G has a much larger funnel, as measured by the distance δ_{ns} , than the bad folder R' . A direct comparison of δ_f for G and R' to that for H is not meaningful because the Hamiltonians and dimensionalities are different. Thus even though δ_f/σ for H is the smallest among the three sequences, its foldability is intermediate.

III. DYNAMICAL CHAOS

In order to study the dynamic chaos we monitor two trajectories that evolve in time from two conformations which

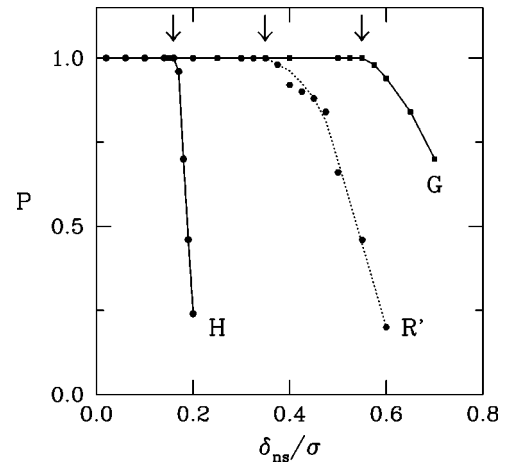


FIG. 3. The dependence of the probability P of falling into the native state as a result of quenching on the distance to the native state. The arrows indicate the values of δ_f . The results are obtained by the Monte Carlo method and are averaged over 100 starting configurations.

are initially separated by a distance ΔR . We chose $\Delta R = 0.001\sigma$. Smaller values of ΔR yield qualitatively similar results. The forces due to the Langevin noise are identical for both trajectories.

Figure 4 illustrates what happens with two initially nearby trajectories as a function of time for systems G , R' , and H , respectively. The trajectories are characterized by the potential energy, radius of gyration R_g , and the number of established native contacts N_c . Two monomers i and j are declared to form a native contact if the distance between them is in the interval $[0.9d_{ij}^N, 1.1d_{ij}^N]$. Independent of which of these quantities is used, we see that the two trajectories quickly come together for system G but continue to be clearly distinct for a much longer time in the case of system R' . System H involves larger scales on the y axis and, on a closer inspection, it behaves like R' .

Figure 5 shows the time dependence of δ at $T=T_{min}$ averaged over many pairs of starting trajectories. The time scales extend to much beyond the folding times. For R' and H the distance δ remains nonzero at these large time scales but for G — $\delta \rightarrow 0$. Thus for good folders all two initially separated trajectories eventually come together. This is not so for bad and intermediate folders. In general, the better the folder, the longer it takes to establish the asymptotic behavior in δ . We can rephrase it by stating that R' is more chaotic than H because the asymptotic large separation between the trajectories is established sooner.

Figure 5 refers to trajectories that start in unfolded conformations. It is interesting to consider what happens when the starting conformations come from a closer neighborhood of the native state. We generate such starting ‘‘points’’ by evolving a trajectory from an unfolded conformation to various stages characterized by predefined values of δ_{ns} . At each state, we spawn a nearby companion trajectory which is displaced by ΔR from the current conformation of the leading trajectory. The stages can alternatively be characterized by the numbers of established native contacts but the δ_{ns} is more convenient to use when one deals with long heteropolymers.

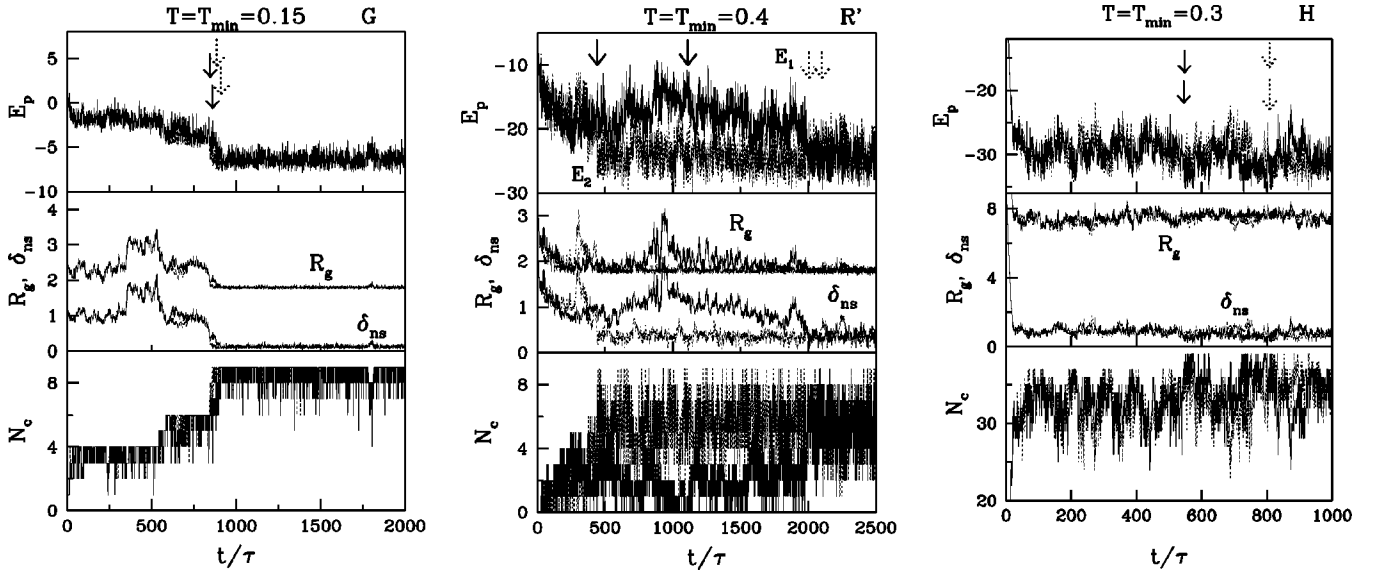


FIG. 4. Time evolution of the potential energy E_p , the gyration radius R_g , the distance to the native state δ_{ns} , and the number of native contacts N_c for two typical trajectories which have the initial departure $\Delta R = 0.001$. The left-hand, center, and right-hand parts of the figure correspond to sequences G , R' , and H , respectively, and all data refer to $T = T_{min}$. The first and second trajectories are denoted by solid and dotted lines, respectively. The left arrow indicates when the last native contact appears for the first time, and the right arrow indicates when folding takes place, i.e., $\delta_{ns} < \delta_c$.

The first panel in the left-hand part of Fig. 6 shows the time dependence of δ for G at $T = 0.1, 0.15$, and 0.2 for times significantly shorter than those corresponding to Fig. 5. It is interesting to point out that the short time behavior of δ_{ab} may yield information about the size of the folding funnel. This can be achieved by studying two initially nearby trajectories which start at various locations in the folding funnel, i.e., at various distances δ_{ns} away from the native state, as illustrated in Fig. 6. Notice that the initial placement affects the character of the initial evolution of δ . For $\delta_{ns} > \delta_{ns}^{th} = 0.55\sigma$ and $T = T_{min} = 0.15$ (the first panel of Fig. 6), the two trajectories diverge. Otherwise, they reduce their relative

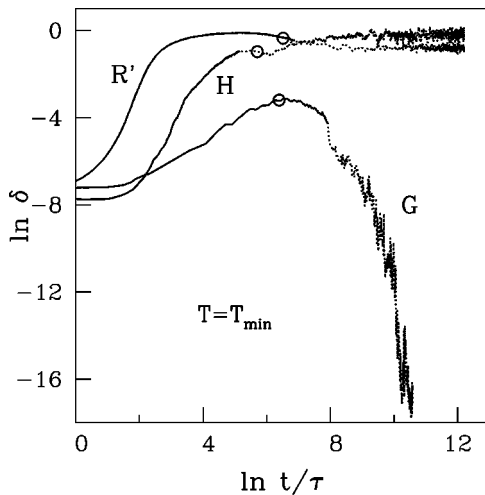


FIG. 5. The time dependence of δ for G , H , and R' at $T = T_{min}$ for two nearby trajectories which start at two nearby unfolded conformations. The solid portions of the curves are averaged over 1000 to 1500 pairs of such trajectories. The dotted portions are averaged over 20 to 200 pairs. The circles indicate values of the median folding times.

distance. This can be interpreted as a situation in which the twin trajectories are placed within the folding funnel. Thus the threshold value of δ_{ns} under the optimal folding conditions should be a measure of size of the folding funnel. In fact, this threshold value agrees with the funnel size as determined from Fig. 3. For temperatures above T_{min} the kinetic conditions deteriorate, the funnel disintegrates, and the threshold behavior in chaos disappears: the system becomes more chaotic. Below T_{min} , on the other hand, the funnel also fades away but the system is close to the quenching conditions. As the system evolves it becomes driven by energy minimization so the trajectories start to come closer together right away even for substantial values of δ_{ns} .

The center and right-hand parts of Fig. 6 show results of a similar analysis for systems R' and H , respectively. For bad folders, even if the trajectories start approaching each other at low T , as it happens for H (the bottom right-hand panel of Fig. 6), they do not meet asymptotically because it is unlikely that they will be simultaneously in the same energy valleys. H displays some borderline behavior but there is no threshold behavior in system R' at any temperature: a viable folding funnel never forms. For good folders, however, studying twin trajectories allows one to establish the geometry of the folding funnel.

In the case of R' , for $T = 0.2$, the time dependence of δ is qualitatively the same as for $T = T_{min} = 0.4$. The qualitative change is observed, however, at $T = 0.1$. Namely, the apparent decrease of the distance is seen for $\delta_{ns}^{th} = 0.4\sigma$. It should be noted that the difference between the good folder G and the bad folder R' is clearly seen only at T_{min} . Away from T_{min} they may behave qualitatively in the same way.

IV. TIME EVOLUTION OF THE POTENTIAL ENERGY

In order to understand the difference in the chaotic behavior of good and bad folders better we consider the time de-

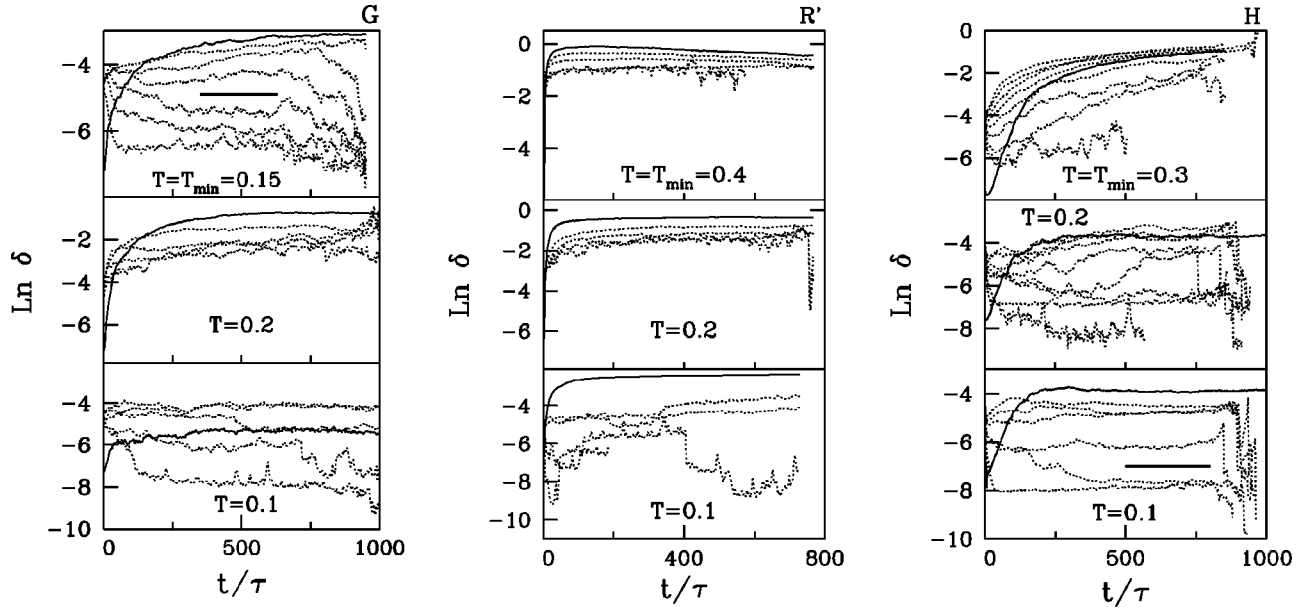


FIG. 6. The time dependence of δ for various types of starting configurations at temperatures which are indicated. The left-hand, center, and right-hand parts correspond to sequences G , R' , and H , respectively. For each T , the initial separation between two trajectories is $\Delta R = 0.001\sigma$. The solid line corresponds to the unfolded starting configuration. *Sequence G*: For $T = T_{min} = 0.15$ the dotted lines correspond to $\delta_{ns} = 0.75, 0.6, 0.55, 0.5, 0.35$, and 0.2σ from top to bottom, respectively. The curve with $\delta_{ns}^{th} = 0.55\sigma$ has a threshold character in the sense that for $\delta_{ns} > \delta_{ns}^{th}$ distance δ decreases with time monotonically. The bar separates two different types of behavior of δ . For $T = 0.2$, the dotted lines correspond to $\delta_{ns} = 0.7, 0.5, 0.3$, and 0.05σ from top to bottom, respectively. In the case of $T = 0.1$ the dotted lines are arranged in order $\delta_{ns} = 1.6, 1.3, 1.1, 0.8$, and 0.5σ . For $T = 0.2$ the distance between two trajectories grows for any δ_{ns} . *Sequence R'*: For $T = T_{min} = 0.4$ the dotted lines correspond to $\delta_{ns} = 0.8, 0.6, 0.4$, and 0.05σ from top to bottom, respectively. For $T = 0.2$, the dotted lines are arranged in the order $\delta_{ns} = 0.8, 0.6, 0.4$, and 0.2σ . For $T = 0.1$ the order is $\delta_{ns} = 0.8, 0.7, 0.6$, and 0.4σ . *Sequence H*: For $T = T_{min} = 0.3$ the dotted lines correspond to $\delta_{ns} = 2, 1.5, 1.2, 1, 0.8, 0.6, 0.4, 0.3$, and 0.15σ from top to bottom, respectively. For $T = 0.2$ the dotted lines correspond to $\delta_{ns} = 1.2, 1, 0.8, 0.6, 0.5, 0.4, 0.2$, and 0.1σ . For $T = 0.1$ the dotted lines correspond to $\delta_{ns} = 1.5, 1.2, 1.0, 0.8, 0.6, 0.5, 0.4$, and 0.2σ . The results are averaged over 500–3000 starting configurations.

pendence of the potential energy E_p on individual trajectories under the optimal folding conditions, i.e., at T_{min} . We consider folding and unfolding trajectories separately and demonstrate that the corresponding properties of E_p are distinct.

The first question we ask is what are the properties of the power spectra of E_p . Figure 7 shows the frequency dependence of $|E_p(\omega)|^2$, where

$$E_p(\omega) = \frac{1}{2\pi} \int \exp(i\omega t) E_p(t) dt. \quad (4.1)$$

The first observation is that if E_p is viewed as noise then this noise is clearly correlated — there is no frequency regime which would correspond to white noise. In other words, if

$$|E_p|^2 \sim \omega^{-s} \quad (4.2)$$

then the exponent s is nonzero. For each of the systems studied we observe two regimes with a power-law dependence on ω : the low- and high-frequency regimes which are separated by $\omega_0 \sim 0.032/\tau$ which corresponds to a time scale of about 200τ . The values of the power-law exponent are indicated in the figure. For system G there is also an intermediate time scale in the folding trajectories where $s = 1.20 \pm 0.20$. It is possible that the existence of the intermediate-frequency regime is a signature of a good foldability in general.

The high-frequency behavior corresponds to a large exponent in the power law, of order 5–7 (the error bars here are of order 0.5). The low frequency, i.e., long time behavior, however, is clearly distinct for G and almost the same for R' .

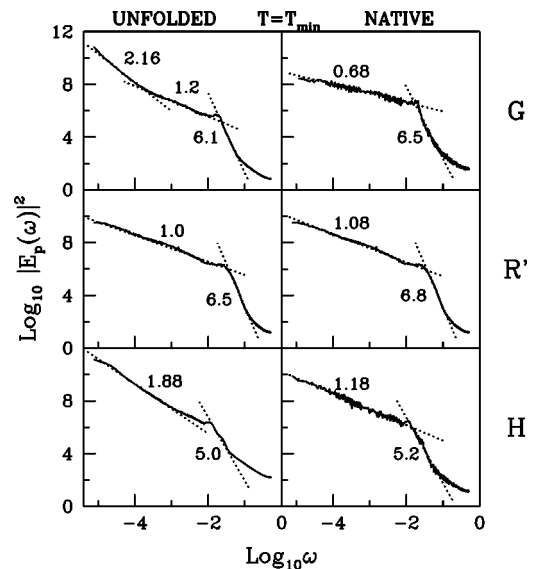


FIG. 7. Spectrum of the potential energy for G , R' , and H at T_{min} . The starting conformations are either unfolded or native as indicated at the top of the figure. The results are averaged over 400 trajectories. The values of f are shown next to the curves.

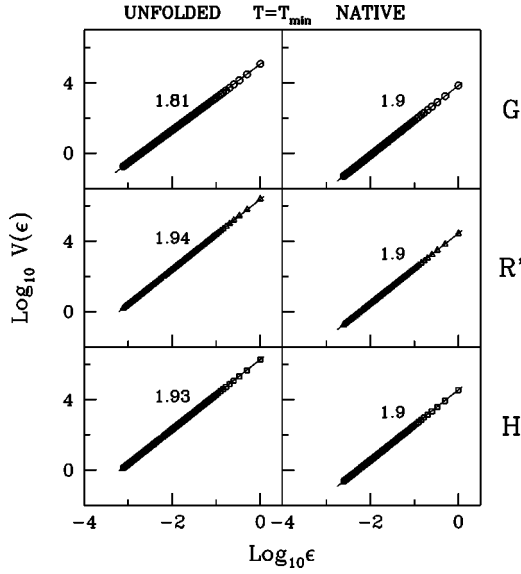


FIG. 8. Dependence of $V(\epsilon)$ on ϵ for G , R' , and H . The results are obtained at $T=T_{min}$. The left- and right-hand panels are for folding and unfolding conformations, respectively. The time steps are equal to the folding times at $T=T_{min}$. The values of γ are shown next to the data points.

For G , the low-frequency behavior of E_p corresponds to $f = 2.16 \pm 0.20$ and 0.68 ± 0.2 for the folding and unfolding trajectories, respectively. For R' , on the other hand, one gets the $1/f$ noise for both kinds of trajectories. This clearly indicates a lack of any folding direction in R' . System H has an intermediate behavior again: for the low-frequency folding trajectories $s = 1.88 \pm 0.24$ and for the unfolding trajectories $s = 1.18 \pm 0.20$. Thus there is a difference between folding and unfolding but the difference is not as strong as for G .

Another way to characterize trajectories has been recently proposed by Lidar *et al.* [14] and it involves determination of the fractal dimensionality γ , which relates to the self-affinity properties of the $E_p(t)$ curve. This fractal dimensionality may be obtained by the ϵ -variation method developed by Dubuc *et al.* [15]. Typically, for any function g one can introduce its ϵ variation $V(\epsilon, g)$ as follows:

$$V(\epsilon, g) = \int_0^1 v(x, \epsilon) dx, \quad (4.3)$$

where the ϵ variation is

$$v(x, \epsilon) = \sup_{x' \in R_\epsilon(x)} g(x') - \inf_{x' \in R_\epsilon(x)} g(x'), \quad (4.4)$$

$$R_\epsilon(x) = \{s \in [0, 1]; |x - s| < \epsilon\}.$$

Figure 8 shows the ϵ dependence of ϵ variation $V(\epsilon)$ for $E_p(t)$ of three typical trajectories at T_{min} run in the folding or unfolding modes. In the folding mode, the trajectories are evolved until the folding is accomplished. In the unfolding mode, the trajectories are analyzed for a duration of a typical median folding time at T_{min} . The slopes in Fig. 8 give the values of γ . If the starting conformation is native then γ appears to be system independent and equal to about 1.90. This again indicates a correlated behavior since for Gaussian distributed numbers $\gamma=2$. On the other hand, if the starting

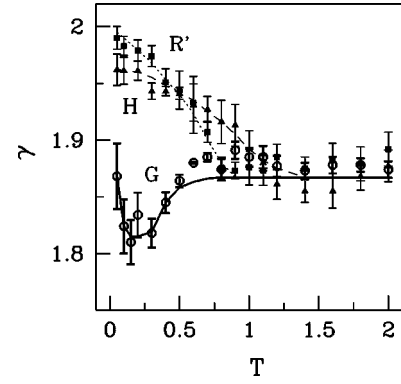


FIG. 9. Temperature dependence of γ for G (open circles), R' (closed squares), and H (closed triangles). The starting conformations are unfolded. The time steps are equal to the folding times at $T=T_{min}$. The number of starting configurations is 20–100.

conformation is unfolded, then $\gamma \approx 1.81$, 1.94, and 1.93 for G , R' , and H , respectively. This suggests that the smaller the γ the better the foldability (and less chaos).

From Figs. 7 and 8 one can see that s has a stronger system dependence compared to γ . This is due to the fact that the spectral and roughness properties refer to different aspects of the behavior. This may be seen clearly in the case of the white noise where $\gamma=2$ but $s=0$ which means that the white noise is not correlated but its profile remains rough. In other words the spectral analysis provides information about the pattern correlation whereas the fractal dimensionality relates to the roughness. Therefore, γ and s may depend on the system in a different way. It is interesting to ask why the system dependences of s and γ in the folding mode are stronger compared to the unfolding mode. The reason seems to be that the time dependence of the potential energy in the folding mode (shown in Fig. 4) is substantially stronger than in the unfolding mode for all of the three sequences. Thus, in the unfolding case the system dependence becomes weaker and γ even loses the dependence entirely. It would be interesting to know if this observation is still valid in real proteins.

The temperature dependence of γ for three sequences is shown in Fig. 9 where the starting conformations are unfolded. The values of γ presented in this figure fulfill the relation $\gamma=2-\alpha$, where α is the roughness exponent [14] if α is determined directly. Studies of models of real proteins [14] indicate that γ may depend on T weakly. This is also true for our model systems as shown in Fig. 9. Note that system H again behaves in a way which is intermediate between R' and G . Interestingly, in the proteinlike sequence G we observe a dip in γ around T_{min} . A similar but wider dip was also observed for real proteins like myoglobin, BPTI and PPT [14]. The presence of the dip could be explained in the following way: around T_{min} the system establishes a folding funnel and the motion becomes less rugged or less chaotic. Thus, fractal analysis around T_{min} may provide useful information about the foldability. It should be noted that our results have been obtained for times equal to the folding times at T_{min} and the related conclusions are valid on these time scales. Longer or shorter runs may, in principle, change

the estimates of γ [14]. Within the error bars, the results shown in Fig. 9, however, do not change if the time scale is doubled.

In conclusion, we have studied the dynamic chaos of several model sequences and demonstrated that good folders are essentially nonchaotic and bad folders are intrinsically chaotic. The energy landscape of heteropolymers can be charac-

terized by the spectral and fractal properties of the time evolution of the potential energy of the system.

ACKNOWLEDGMENTS

We thank T. X. Hoang for useful discussions and technical help. This work was supported by Komitet Badan Naukowych (Poland; Grant No. 2P03B-146 18).

-
- [1] A. J. Bray and M. A. Moore, Phys. Rev. Lett. **58**, 57 (1987).
 - [2] M. Vendruscolo, A. Maritan, and J. R. Banavar, Phys. Rev. Lett. **78**, 3967 (1997).
 - [3] H. J. Bussemaker, D. Thirumalai, and J. K. Bhattacharjee, Phys. Rev. Lett. **79**, 3530 (1997).
 - [4] R. A. Broglia, G. Tiana, H. E. Roman, E. Vigezzi, and E. I. Shakhnovich, Phys. Rev. Lett. **82**, 4727 (1999).
 - [5] V. S. Pande, A. Y. Grosberg, and T. Tanaka, Folding Des. **2**, 109 (1997).
 - [6] A. R. Fersht, Curr. Opin. Struct. Biol. **5**, 79 (1994).
 - [7] M. S. Li and M. Cieplak, Phys. Rev. E **59**, 970 (1999).
 - [8] M. S. Li and M. Cieplak, J. Phys. A **32**, 5577 (1999).
 - [9] T. X. Hoang and M. Cieplak, J. Chem. Phys. **112**, 6851 (2000).
 - [10] M. P. Allen and D. J. Tildesley, *Computer Simulation of Liquids* (Oxford University Press, New York, 1987).
 - [11] N. Go and H. Abe, Biopolymers **20**, 991 (1981).
 - [12] C. J. Camacho and D. Thirumalai, Proc. Natl. Acad. Sci. USA **90**, 6369 (1993).
 - [13] N. D. Socci and J. N. Onuchic, J. Chem. Phys. **101**, 1519 (1994).
 - [14] D. A. Lidar, D. Thirumalai, R. Elber, and R. B. Gerber, Phys. Rev. E **59**, 2231 (1999).
 - [15] B. Dubuc, J. F. Quiniou, C. Roques-Carmes, C. Tricot, and S. W. Zucker, Phys. Rev. A **39**, 1500 (1989).
 - [16] G. Iori, E. Marinari, and G. Parisi, J. Phys. A **24**, 5349 (1991).